Extraction of neutron densities from elastic proton scattering by ^{206,207,208}Pb at 650 MeV

V. E. Starodubsky and N. M. Hintz
School of Physics and Astronomy, University of Minnesota, Minneapolis, Minnesota 55455
(Received 30 August 1993)

The method for extraction of neutron and matter densities from data on cross sections and spin observables for elastic p-nucleus scattering is presented. The effective nuclear potential was treated to the first order with respect to the t-matrix and density distributions. To eliminate uncertainties associated with the t matrix, the latter has been determined directly from p-^{40}Ca scattering data, where the proton and neutron densities are known sufficiently well. The medium modifications in the t matrix have been included by means of density dependent terms added to the free t matrix. The neutron densities to be found were expressed as a Hartree-Fock (HF) distribution plus a small correction expanded in a Fourier-Bessel series with inclusion of only low-frequency components determined by the data. High-frequency components are presented by the HF term. Expressions for the physical observables were linearized in terms of the expansion coefficients, the latter being determined through an iterative procedure from the χ^2 criterium. The method enables one to obtain statistical fluctuations in those Fourier components as they are generated by experimental error bars. The normalization and model uncertainties have been also estimated. The extracted densities of ^{206,207,208}Pb and their differences were compared with the HF results calculated by us with the Skyrme interaction. On the whole, pretty good agreement has been achieved.

PACS number(s): 21.10.Gv, 25.40.Cm, 21.30.+y, 27.80.+w

I. INTRODUCTION

Substantial progress has been made in recent years in studies of nuclear structure with electron and proton scattering at intermediate energies. In particular, elastic electron scattering (especially in combination with muonic x-ray data) provides precise information on charge distributions $\rho_{\rm ch}(r)$ in the nuclear ground state [1,2]. It has become possible, due to experimental achievements allowing measurements to very high momentum transfer ($q \simeq 3.5$ fm^{-1}) [3], and to theoretical developments [4–7], to obtain model independent charge distributions with statistical error bands generated by experimental error bars. In some cases [3] overall uncertainties were reported to be as small as 1–2% in the nuclear interior. In elastic electron scattering the dominant contribution comes from the nuclear static Coulomb potential generated by $\rho_{\rm ch}(r)$. The remarkable simplicity of this interaction is a key factor allowing such accurate determination of $\rho_{\rm ch}(r)$.

In the case of elastic proton scattering the nuclear structure is presented mainly by the single-particle density distributions of both protons $\rho_p(r)$ and neutrons $\rho_n(r)$. The overall contribution of two-body density terms coming from dispersion and correlation corrections has been shown to be small, due to a significant compensation between them [8,9].

The dominant contribution of single-particle terms makes the elastic proton-nucleus (pA) scattering very attractive for the purposes of determination of $\rho_n(r)$, the proton density $\rho_p(r)$ being taken from other sources, e.g., elastic electron scattering.

In nuclei with equal numbers of protons Z and neutrons N, the neutron and proton densities are close to each other. However, in the case $N \neq Z$, the densities $\rho_n(r)$ and $\rho_p(r)$ may differ very substantially (besides the trivial change of the normalization). This follows very clearly from results of modern self-consistent microscopic approaches such as Hartree-Fock (HF) [10,11] or the quasiparticle Lagrange method (QLM) [12,13]. As compared to what one has for the proton densities, the experimental information on $\rho_n(r)$ is generally scarce and they are poorly known in nuclei with $N \neq Z$. To a considerable extent this is a consequence of a poor knowledge of the NN-scattering amplitudes in medium or equivalently t matrices and the strong absorption mechanism. These uncertainties are a major obstacle hindering attempts to obtain information on $\rho_n(r)$ comparable in quality to that known for the charge densities. Due to the strong absorption of protons, the nuclear interior is not well probed as in the case of electron scattering. At 650 MeV, the imaginary part of the optical potential Im$V_{\rm opt}$ in the inner region of ^{208}Pb is about 46 MeV. This causes substantial suppression of the incident proton wave, hindering a deep penetration inward. However, due to a remarkable constancy of the isoscalar matter density in the nuclear interior, the distortion factors are weakly position dependent, and can be taken outside. These overall multiplicative factors reduce the cross section considerably, but they, in themselves, do not complicate the picture. This circumstance is similar to what occurs in the quasifree reactions such as $(p,2p)$ and $(e,e'p)$. There, an exact determination of the momentum distributions of the bound nucleons is possible only in the plane-wave

limit. Nevertheless, the former can also be obtained with good accuracy in a more realistic situation with the absorption factors included. This is because the main effect produced by the distortion is an overall reduction of the cross sections with only little change in the plane-wave momentum distributions [14]. In this respect, the description resembles the weak coupling limit.

It is evident that obtaining quantitative and detailed information on the spatial distribution of neutrons in the nuclear ground state is a problem of major importance. In this paper we address this problem by analyzing new data on cross sections and analyzing power for elastic proton scattering by ^{206,207,208}Pb at 650 MeV measured in LAMPF experiment E855 [15]. The lead region is of particular interest both theoretically and experimentally for many reasons. These are the heaviest stable nuclei and are very sensitive to the saturation of nuclear forces. Most theoretical approaches are best valid for spherical doubly closed nuclei. Many electron and proton scattering data at different energies have been obtained in this region which thus provides a good basis for critical analysis. Furthermore, the examination of data for neighboring isotopes enables one to study relative effects in densities arising from addition of one or two particles (or holes). Such relative measurements can be done with higher accuracy than absolute measurements for a single nucleus.

In order to avoid uncertainties associated with incomplete knowledge of the in-medium t matrices, we decided to determine them directly from experiment [16]. Thus, we used a two-step procedure to untangle the knot of unknown t matrices and neutron densities. First, we analyzed data for elastic proton scattering at 650 MeV on ^{40}Ca [17], where the neutron density was taken quite reliably as the sum of unfolded experimental charge density and a small correction term calculated theoretically. We determined the isoscalar component of the effective amplitude from a best fit search procedure. The amplitude we used differs from the free t matrix of Franey and Love [18] by the presence of additional density dependent terms with some adjustable parameters (two in each component of the amplitude). The form of the ρ dependence we chose was motivated to a certain extent by the ideas of Brown and co-workers [19,20] on the universal renormalization of meson masses in the nuclear medium. Given the NN-scattering amplitudes determined from the analysis of ^{40}Ca, the next step was to obtain the neutron densities from data (cross sections and analyzing powers) on elastic proton scattering by the lead isotopes.

To extract the neutron densities we extended the approach of Friar and Negele [21] proposed originally for the determination of charge densities from the analysis of elastic electron scattering and muonic transition energies to the case of elastic proton scattering. This method, in slightly modified fashion, has been examined in Ref. [22] in the context of Glauber multiple scattering theory. Another approach based on Sick's method [6] was used in Ref. [23].

We searched the neutron densities in the form $\rho_n(r) = \rho_n^0(r) + \delta\rho_n(r)$, where $\rho_n^0(r)$ and $\delta\rho_n(r)$ are the main and correction terms, respectively. The $\delta\rho_n(r)$ term was expanded in a Fourier-Bessel (FB) series. The number of coefficients was mostly specified by the maximum momemtum transfer $q_{\max}$ which was 2.91 fm^{-1} in our case. For $\rho_n^0(r)$ we used the Hartree-Fock (HF) densities calculated here with the Skyrme interaction SkM′ [10] and pairing included. Since the $\delta\rho_n(r)$ term was treated as a small correction, we expanded the cross section and spin observables in a series with regard to $\delta\rho_n(r)$ and kept linear terms. Thus, the condition for the minimum of the χ^2 value resulted in a system of linear equations for the expansion coefficients and could be solved easily. The whole procedure was repeated by redefining $\rho_n^0(r)$ as $\overline{\rho}_n^0 = \rho_n^0(r) + \delta\rho_n(r)$ to determine a new $\delta\overline{\rho}_n$ at the next iteration, and so on until a required accuracy was achieved. Statistical errors of the data were projected into the final results in the form of statistical error bands for the densities and their relative differences. Those error envelopes show how the corrections $\delta\rho_n(r)$ (which, by definition, contain only low Fourier component determined by the data) fluctuate due to the experimental statistical errors. High-frequency terms, introduced with the HF model, do not contribute to the statistical error bands. The results for the neutron and matter densities and their differences were also compared with predictions of the HF theory mentioned above.

II. BASIC APPROXIMATIONS FOR THE OPTICAL POTENTIAL AND t MATRIX

According to current general thinking, a very appealing approach to describe nuclear phenomena and scattering processes in particular would be one based on an effective Lagrangian derived from QCD with effective nucleonic and mesonic degrees of freedom. However, the theory at such a level has not yet been developed. Therefore less rigorous approaches including some phenomenological quantities have been examined. Some years ago theoretical descriptions of elastic (pA) scattering based on the relativistic impulse appproximation (RIA) for the Dirac equation [24] and another one [25] deduced from covariant meson exchange theory (IA2) were proposed. Predictions of these relativistic models were mostly successful for polarization data below 500 MeV, the IA2 theory doing somewhat better below 400 MeV but worse than RIA at 500 MeV. For differential cross sections these relativistic approaches did not always provide an improvement in comparison with nonrelativistic (NR) multiple scattering theories, in many cases doing even worse. Furthermore, there was not observed any systematic improvement with the increase of incident proton energy up to 1 GeV even for the case of polarization data as one might expect [17,26].

In recent years considerable progress has been made in the NR multiple scattering theory to include off-shell, full-folding, and medium modification effects [27–29]. These corrections to the single-scattering term of the optical potential improve the NR description of the experiment. On the other hand, for our purpose of studying the neutron densities, cross section data are to a certain degree more important than data for spin observables. Keeping in mind those reasons, we chose the NR de-

scription of the elastic (pA) scattering based upon the Schrödinger equation using relativistic kinematics.

As was mentioned briefly in the Introduction, the nuclear optical potential at energies near 1 GeV can be approximated with good accuracy by its first-order term of the structure ($t\rho$), where t and ρ are the two-body t matrix and one-body density, respectively. The second-order term being proportional to the pair correlation function is generally small, due to a significant compensation between contributions from correlations of short and long ranges [8,9]. Using the free two-body t matrix in the leading first-order term is called the impulse approximation (IA). Thus, a basic requirement for the IA is the vanishing influence of the medium in intermediate states.

Numerous calculations have shown that the IA provides a good description of the elastic (pA) cross sections near 1 GeV [26,30,31]. However, it fails at lower energies. Corrections to the IA due to off-shell, full-folding, and in-medium effects on the free t matrix should be included. Evaluations of the t matrix modified by the nuclear environment were performed by using the Brueckner G matrix [29,32] calculated for energies near 300 MeV or by the Watson τ matrix [33] which includes binding effects only for target nucleons [28]. Although results of the three mentioned approaches are in a qualitative agreement predicting a repulsive contribution for the real central t matrix, they differ substantially on a quantitative level. This would result in big variations for scattering quantities such as cross sections and spin observables. Obviously, some more work is required in this direction as well as in studies of the second-order correlation terms at energies of a few hundred MeV. Taking into account the reasons outlined above, we adopted an approach in which all those corrections to the IA are included phenomenologically in an effective t matrix. Its isoscalar part was determined from the p-^{40}Ca scattering data for cross section [17], and spin observables [34], the neutron density being taken as

$$\rho_n(r) = \rho_p(r) + [\rho_n^{\rm HF}(r) - \rho_p^{\rm HF}(r)] \ . \tag{1}$$

Here, the point proton density $\rho_p(r)$ was obtained by unfolding the experimental charge density of Ref. [35] with the neutron contribution included [36], and the correction term was calculated by us in the HF approximation with the Skyrme interaction SkM′.

Thus, the folded optical potential $V(r)$ which was used in the Schrödinger equation contained the Coulomb V_Z, central V_C, and spin-orbit $V_{\rm LS}$ terms of the following structure:

$$V(r) = V_Z(r) + V_C(r) + V_{\rm LS}(r)(\boldsymbol{\sigma}\cdot\boldsymbol{l}) \ , \tag{2}$$

$$V_Z(r) = e^2 \int d^3\mathbf{r}' \rho_{\rm ch}(\mathbf{r}')/|\mathbf{r}-\mathbf{r}'| \ , \tag{3}$$

$$V_C(r) = \frac{2}{\pi} \sum_{i=n,p} \int q^2 dq j_0(qr) \eta t_C^i(q,\rho(r))\rho_i(q) \ , \tag{4}$$

$$V_{\rm LS}(r) = \frac{2}{\pi}\frac{1}{r}\frac{d}{dr} \sum_{i=n,p} \int q^2 dq j_0(qr) \eta \tau_{\rm LS}^i(q,\rho(r))\rho_i(q) \ , \tag{5}$$

where $\rho(r) = \rho_n(r) + \rho_p(r)$. A kinematic factor η [18] relates the t matrix in the nucleon-nucleus frame to that in the nucleon-nucleon frame $t(q)$. The latter was presented in the form

$$t(q) = t_C(q) + i t_{\rm LS}(q)(\boldsymbol{\sigma}\cdot\boldsymbol{n}) \ , \tag{6}$$

where $\mathbf{n}$ is the normal to the scattering plane. The auxiliary quantity $\tau_{\rm LS}(q)$ [16] is related to $t_{\rm LS}(q)$ by the relationship

$$t_{\rm LS}(q) = -kq\sqrt{1-\left(\frac{q}{2k}\right)^2}\,\tau_{\rm LS}(q) \ , \tag{7}$$

in which k is the incident proton momentum in the (pA) center-of-mass system, and q is the momentum transfer.

Our choice of the form of the effective t matrix was motivated to an extent by Brown's idea on the universality of meson and nucleon mass renormalization in the nuclear medium. It was argued in Refs. [19,20] that meson masses should scale inside nuclei in the same proportion as the nucleon mass does. The principal in-medium scaling ansatz conjectured in Ref. [19] is

$$\frac{m_\sigma^*}{m_\sigma} = \frac{m_\rho^*}{m_\rho} = \frac{m_\omega^*}{m_\omega} = \frac{m_N^*}{m_N} \ , \tag{8}$$

where m_σ, m_ρ, and m_ω, are the masses of σ, ρ, and ω mesons and m_N is the nucleon mass, the asterisk denoting the in-medium density dependent quantities.

In nuclear structure theories such as the HF method with a nonlocal NN effective interaction [37,38], one has

$$\frac{m_N}{m_N^*(r)} = 1 + \lambda\frac{\rho(r)}{\rho_0} \ , \tag{9}$$

where a typical value of λ is 0.2 ± 0.1, and ρ_0 is the nuclear matter density. The first results indicating the necessity of meson mass scaling for proton scattering cross sections have been presented in Refs. [39–41].

Now, if we adopt the Yukawa form for the effective t matrix and treat corresponding meson mass (range) parameters as the ones subjected to the scaling law, we can expand the interaction in a series with respect to λ. More specifically, assuming a Yukawa form similar to that proposed by Franey and Love [18] for the free t matrix we can obtain a somewhat complicated structure for the ρ-dependent terms. Taking into account that the change of meson masses is not the only cause of medium modifications (e.g., restrictions due to the Pauli principle can be significant) and intending to simplify somewhat the expansion expressions, we have chosen the following parametrization for the isoscalar effective t matrix:

$$\mathrm{Re}[t_C(q,\rho)] = a_1 \mathrm{Re}[t_C^0(q)] + a_2\frac{\rho}{\rho_0}\left[1+\left(\frac{q}{\mu_1}\right)^2\right]^{-2} \ , \tag{10}$$

$$\mathrm{Im}[t_C(q,\rho)] = a_3 \mathrm{Im}[t_C^0(q)] + a_4 \frac{\rho}{\rho_0}\left[1+\left(\frac{q}{\mu_2}\right)^2\right]^{-2}, \tag{11}$$

$$\mathrm{Re}[\tau_{\mathrm{LS}}(q,\rho)] = a_5 \mathrm{Re}[\tau_{\mathrm{LS}}^0(q)] + a_6 \frac{\rho}{\rho_0}\left[1+\left(\frac{q}{\mu_3}\right)^2\right]^{-3}, \tag{12}$$

$$\mathrm{Im}[\tau_{\mathrm{LS}}(q,\rho)] = \mathrm{Im}[\tau_{\mathrm{LS}}^0(q)]\,. \tag{13}$$

Here t_C^0, t_{LS}^0 are the central and spin-orbit free t matrices of Franey and Love [18], a_i $(i = 1-6)$ are the adjustable parameters, and $\rho_0 = 0.1589$ fm^{-3} is the nuclear matter density.

The parameters μ_1, μ_2, and μ_3 were not varied during the χ^2 search procedure. The sensitivity to their values is not strong, especially for μ_2 and μ_3. The μ_1 parameter determines mostly the ratio of real to imaginary parts of the t matrix at $q \leq 1$ fm^{-1} thus influencing differential cross sections at their minima. Their values were chosen to be $\mu_1 = 1.2$ fm^{-1}, $\mu_2 = 2.0$ fm^{-1}, $\mu_3 = 6.0$ fm^{-1}. According to Ref. [28], the ρ dependence of $\mathrm{Im}[\tau_{\mathrm{LS}}(q,\rho)]$ is very weak at 650 MeV for momentum transfers within the range $0 \leq q \leq 3$ fm^{-1}. Therefore, we have neglected it.

Expressions (10)–(13) for $t(q,\rho)$ are somewhat different from those proposed in Ref. [16]. The difference is in the form of $\mathrm{Im}[t_C(q,\rho)]$ and in the values of powers of the denominators in Eqs. (10)–(13). Because of the expansion with respect to λ of the Yukawa potential, the values of the powers are greater by 1 as compared to those used in Ref. [16]. The $\mathrm{Im}[t_C(q,\rho)]$ of Ref. [16] contained a special damping factor introduced explicitly to implement the expected behavior caused by Pauli blocking. In Eqs. (10)–(13) the forms of the real and imaginary parts of $\tau_C(q,\rho)$ are identical. This parametrization is compatible with the anticipated depletion of the imaginary part as has been found in our best fit solution.

III. METHOD OF DETERMINATION OF THE NEUTRON DENSITIES FROM ELASTIC (pA) SCATTERING DATA

It is evident that there is no way to extract the spatial distribution of neutron densities in a complete and truly exact form even in the case of zero statistical and systematic experimental errors. This is clearly seen in the first-order Born approximation, where the scattering amplitude is proportional to the Fourier transform of the density. As long as measurements are restricted by a maximum momentum transfer $q_{\max}$, it is not possible to invert exactly the expression for the amplitude. One can never exclude high Fourier components with the wavelength $\lambda < 2\pi/q_{\max}$. In other words, since the data are not sensitive to these frequencies, it is always possible to add a rapidly oscillating function (with $\lambda < 2\pi/q_{\max}$) to any physically reasonable density $\rho(r)$ without a substantial deterioration of χ^2. This implies that $\rho(r)$ at any r is not well determined by the real data. In this situation, one must formulate model constraints on the density based on physical considerations.

One of them is that the resulting density fluctuations should not have a wavelength less than $\lambda_{\min} = \pi/k_F \simeq 2.36$ fm (k_F is the Fermi momentum) [21]. One also knows that densities should decay exponentially in the surface in accordance with the damping law of single-particle wave functions. In the LAMPF experiment E855, the maximum momentum transfer was $q_{\max} = 2.91$ fm^{-1}, which corresponds to $\lambda = 2\pi/q_{\max} = 2.16$ fm thus providing the possibility of measuring the expected density fluctuations.

Our strategy is to use the theoretical HF neutron densities $\rho_n^0(r)$ as a starting approximation and to correct only those features of $\rho_n^0(r)$ which are actually determined by the data, i.e., the low Fourier components. Then we calculate statistical uncertainties in those corrections which are produced by experimental statistical errors. In a manner similar to Refs. [21,22] we separate the neutron density $\rho_n(r)$ into two terms $\rho_n(r) = \rho_n^0(r) + \delta\rho_n(r)$, where $\rho_n^0(r)$ is normalized to the neutron number N and $\delta\rho_n(r)$ is a small correction. The latter is expanded in the Fourier series in the region $0 \leq r \leq R_0$ and is chosen to have zero normalization. The expansion radius R_0 will be specified later on.

For the inversion problem we are discussing, it is very beneficial to have a statistical independence between the expansion coefficients, which we denote here as C_m. This implies that each coefficient is specified by the data at the corresponding value of q. The analysis of elastic proton scattering at 1 GeV made in Ref. [22] has shown that this condition is satisfied well enough when the phase shifts entering the Glauber amplitude were expanded with respect to the cylindrical Bessel functions. One can expect that under similar circumstances the expansion of $\delta\rho_n(r)$ in a spherical Fourier-Bessel (FB) series would give close results. In the case of electron scattering it was explicitly demonstrated in Ref. [21] that even in heavy nuclei the scattering data essentially specify the Fourier-Bessel transform of $\rho_{\mathrm{ch}}(r)$.

Therefore, we expanded $\delta\rho_n(r)$ as

$$\delta\rho_n(r) = \begin{cases} \sum_{m=1}^{M} C_m j_0(q_m r) & 0 \leq r \leq R_0 \\ 0 & r > R_0\,, \end{cases} \tag{14}$$

where $j_0(q_m r)$ is the spherical Bessel function of zero order, and $q_m = m\pi/R_0$. It makes sense to choose R_0 close to the point where statistical uncertainties in $\delta\rho_n(r)$ corresponding to experimental statistical errors in the scattering data are comparable to the entire density $\rho_n(r)$. In practice this happens at a distance close to $2r_n$, where r_n is the neutron root mean square radius. Hence, for the lead isotopes under consideration $R_0 \simeq 11$ fm. The dependence on R_0 in our final results is weak enough for R_0 being within the range 11–13 fm. Now, recalling that each expansion coefficient is essentially specified

by a datum at certain q, the total number of coefficients M is determined from the condition $q_M = q_{\max}$, i.e., $M = R_0 q_{\max}/\pi \simeq 10$ for $q_{\max} = 2.91$ fm^{-1} attained in the LAMPF experiment E855.

It is clear that an infinitesimal variation $\delta\rho_n$ produces corresponding small changes in the potentials δV_C, $\delta V_{\rm LS}$, the phase shifts $\delta\eta_{l,j\pm1/2}$, cross sections $\delta\sigma$, and in the spin observables δA_y, δQ. It is not difficult to infer perturbation expressions for these quantities which we used in our calculations. First, we recall that with the spin-orbit interaction included the Schrödinger equation separates into a pair of decoupled equations for the radial wave functions $u_l^{\pm}(r)$ corresponding to two possible orientations of spin, the term $\langle \boldsymbol{\sigma}\cdot\boldsymbol{l}\rangle$ being equal to l for $j = l + 1/2$ and $-(\ell+1)$ for $j = l - 1/2$

$$\frac{d^2u_l^+}{dr^2} + \frac{2\mu}{\hbar^2}\left[E - V_Z - V_C - lV_{\rm LS} - \frac{\hbar^2 l(l+1)}{2\mu r^2}\right]u_l^+ = 0 , \tag{15}$$

$$\frac{d^2u_l^-}{dr^2} + \frac{2\mu}{\hbar^2}\left[E - V_Z - V_C + (l+1)V_{\rm LS} - \frac{\hbar^2 l(l+1)}{2\mu r^2}\right]u_l^- = 0 .$$

These equations are solved (for $l = 0$ only the first one is used) to give the phase shifts $\eta_l^{\pm}$ and two scattering amplitudes $A(\theta)$, $B(\theta)$, where

$$A(\theta) = f_C(\theta) + \frac{1}{2ik}\sum_{l=0}^{\infty}\left[(l+1)e^{2i\eta_l^+} + le^{2i\eta_l^-} - (2l+1)\right] \times e^{2i\sigma_l}P_l(\cos(\theta)) , \tag{16}$$

$$B(\theta) = \frac{1}{2ik}\sum_{l=1}^{\infty}\left[e^{2i\eta_l^+} - e^{2i\eta_l^-}\right]e^{2i\sigma_l}P_l^1(\cos(\theta)) , \tag{17}$$

and where $f_C(\theta)$ and σ_l are the Coulomb amplitude and phase shifts, respectively. In terms of $A(\theta)$ and $B(\theta)$ the differential cross section $d\sigma/d\Omega$, the analyzing power $A_y(\theta)$, and the spin rotation parameter $Q(\theta)$ are given by

$$\frac{d\sigma}{d\Omega} = |A|^2 + |B|^2 , \tag{18}$$

$$A_y(\theta) = \frac{2{\rm Im}(AB^*)}{|A|^2 + |B|^2} , \tag{19}$$

$$Q(\theta) = -\frac{2{\rm Re}(AB^*)}{|A|^2 + |B|^2} . \tag{20}$$

For an infinitesimal change $\delta\rho_n$ one can obtain

$$d\sigma = 2{\rm Re}\,(A^*\delta A + B^*\delta B) ,$$

$$\delta A = \frac{1}{k}\sum_{l=0}^{\infty}\left[(l+1)e^{2i\eta_l^+}\delta\eta_l^+ + le^{2i\eta_l^-}\delta\eta_l^-\right]e^{2i\sigma_l}P_l(\cos(\theta)),$$

$$\delta B = \frac{i}{k}\sum_{l=1}^{\infty}\left[e^{2i\eta_l^+}\delta\eta_l^+ - e^{2i\eta_l^-}\delta\eta_l^-\right]e^{2i\sigma_l}P_l^1(\cos(\theta)) ,$$

$$\delta\eta_l^{\pm} = -\frac{2\mu}{\hbar^2 k}\int_0^{\infty} dr\,\delta V_l^{\pm}(u_l^{\pm})^2 ,$$

$$\delta V_l^+ = \delta V_C + l\delta V_{\rm LS} , \tag{21}$$

$$\delta V_l^- = \delta V_C - (l+1)\delta V_{\rm LS} ,$$

$$\delta V_C(r) = \frac{2}{\pi}\int q^2 dq j_0(qr)\eta\left[t_C^n(q,\rho(r)) + \sum_{i=n,p}\rho_i\partial t_C^i/\partial\rho\right]\delta\rho_n(q) ,$$

$$\delta V_{\rm LS}(r) = \frac{2}{\pi}\frac{1}{r}\frac{d}{dr}\int q^2 dq j_0(qr)\eta\left[\tau_{\rm LS}^n(q,\rho(r)) + \sum_{i=n,p}\rho_i\partial\tau_{\rm LS}^i/\partial\rho\right]\delta\rho_n(q) .$$

Expressions for δA_y and δQ in terms of δA and δB can be obtained in a similar way although they are somewhat lengthy.

Equations (21) provide a linear constraint between variations of the observable quantities and $\delta\rho_n$ or equivalently $\{C_m\}$. This linear dependence can be written in the form

$$\sigma(q_\alpha) = \sigma_{0\alpha} + \sum_{m=1}^{M} C_m S_{\alpha m} , \tag{22}$$

where $\sigma_{0\alpha}$ is the cross section generated by the density $\rho_n^0(r)$, and the quantities $S_{\alpha m} = \partial\sigma(q_\alpha)/\partial C_m$ can be evaluated from equations analogous to Eqs. (21) with a substitution of $\delta\rho_n(q)$ by $(2\pi R_0/q_\alpha q_m)[j_0((q_\alpha - q_m)r) - j_0((q_\alpha + q_m)r)]$. Similar expressions can be also written for the spin observables A_y and Q.

To determine the $\{C_m\}$ coefficients we used the χ^2 criterium [42], that is, we found them from the minimum condition for the quantity

$$\chi^2 = \sum_{\alpha=1}^{N_p}(\sigma_\alpha^{\rm exp} - \sigma_\alpha)^2/\epsilon_\alpha^2 , \tag{23}$$

where $\sigma_\alpha^{\rm exp}$ is the experimental value of σ_α and ϵ_α is the

standard deviation at the point q_α. Data for cross sections and spin observables were combined into a total χ^2 sum with N_p data points.

A direct consequence of the linear dependence noted above is that the minimum condition for the χ^2 value results in the system of linear equations for $\{C_m\}$:

$$\sum_{k=1}^{M} b_{ik} C_k = d_i \ , \tag{24}$$

where

$$b_{ik} = \sum_{\alpha=1}^{N_p} S_{\alpha i} S_{\alpha k} / \epsilon_\alpha^2 \ , \tag{25}$$

$$d_i = \sum_{\alpha=1}^{N_p} (\sigma_\alpha^{\rm exp} - \sigma_{0\alpha}) S_{\alpha i} / \epsilon_\alpha^2 \ . \tag{26}$$

Restrictions arising from the requirement of zero normalization for $\delta\rho_n(r)$ can be included into the system (24) by using the Lagrange multipliers technique [21]. This does not change the structure of the system. The latter can be exactly solved by inverting the matrix b_{ik}. Thus

$$C_i = \sum b_{ik}^{-1} d_k \ . \tag{27}$$

By definition, the correlation error in the density is given by

$$D_n(r, r') = \langle [\rho_n(r) - \langle \rho_n(r) \rangle] [\rho_n(r') - \langle \rho_n(r') \rangle] \rangle \ . \tag{28}$$

The statistical error band for extracted neutron density $\Delta\rho_n(r)$ is defined as

$$\Delta\rho_n(r) = \langle [\rho_n(r) - \langle \rho_n(r) \rangle]^2 \rangle^{1/2} \ . \tag{29}$$

It can be expressed in terms of the covariance matrix for the C coefficients

$$\delta^2 C_{kl} = \langle [C_k - \langle C_k \rangle][C_l - \langle C_l \rangle] \rangle \ . \tag{30}$$

For statistically uncorrelated data points the latter is known to be equal to b_{kl}^{-1}, where the matrix b_{kl} is defined in Eq. (25). Thus, one has

$$\begin{aligned} \Delta\rho_n(r) &= \langle [\delta\rho_n(r) - \langle \delta\rho_n(r) \rangle]^2 \rangle^{1/2} \\ &= \sum_{kl} j_0(q_k r) j_0(q_l r) \delta^2 C_{kl} \\ &= \sum_{kl} j_0(q_k r) j_0(q_l r) b_{kl}^{-1} \ . \end{aligned} \tag{31}$$

To provide a better zero-order term $\rho_n^0(r)$ an iterative procedure was carried out. At each ith iteration the main term was redefined as $\rho_n^{0(i+1)} = \rho_n^{0(i)} + \delta\rho_n^{(i)}$ and a new correction $\delta\rho_n^{(i+1)}$ was determined from the χ^2 minimum condition. The entire process was continued until the desired accuracy of convergence was achieved.

For $\rho_n^0(r)$, we used the neutron density obtained for a given nucleus with the HF theory with the Skyrme interaction SkM′ [10] including pairing. That interaction has proved to be very successful in describing various nuclear properties including the ground-state densities. Making use of the FB expansion of the HF densities as $\rho_n^0(r)$ did not result in any significant differences when ten FB coefficients were included and $R_0 = 11$ fm. We will discuss model error associated with the role of higher harmonics neglected in the FB series in the next chapter.

Other input quantities used in the calculations were proton densities. We obtained them by unfolding the charge densities determined from electron scattering [43] and muonic x rays (see also Ref. [44]). Corrections for the neutron charge distribution and the spin-orbit contribution were included [36]. The latter was calculated using proton and neutron spin-orbit densities obtained from the HF method.

IV. RESULTS AND DISCUSSION

A. The effective t matrix

First, we present and discuss computational results for the effective isoscalar t matrix, which was introduced in Sec. II as if the first-order optical potential of the form $(t\rho)$ was the exact approximation. This t matrix is density dependent due to the influence of the medium (role of the Pauli principle, binding and correlation effects in intermediate states, meson mass change). Its central and spin-orbit parts were parametrized as in Eqs. (10)–(13), where the free t matrices $t_C^0(q)$ and $\tau_{\rm LS}^0(q)$ were taken from Ref. [18] for the energy 650 MeV.

Six adjustable parameters a_i $(i = 1 - 6)$ were determined from the best fit procedure providing a minimum value of χ^2. The latter included data for p-^{40}Ca elastic scattering cross sections [17], analyzing power, and spin rotation parameter [34] at 650 MeV. The ^{40}Ca nucleus has been chosen for that purpose because the condition $Z = N$ in combination with sufficiently small contribution from the Coulomb potential provides a closeness of the neutron and proton density distributions.

The point proton density $\rho_p(r)$ of ^{40}Ca, which was an input quantity in this calculation, was obtained by unfolding the corresponding charge density [35] including the neutron charge contribution [36].

The external parameters μ_1, μ_2, and μ_3 were not varied during the χ^2 search. The sensitivity of final χ^2 values to the magnitudes of μ_2 and μ_3 was found to be fairly weak. The values of these two parameters $\mu_2 = 2.0$ fm^{-1} and $\mu_3 = 6.0$ fm^{-1} were chosen to be equal to the values of μ_1 and μ_3 of Ref. [16], respectively. The sensitivity to μ_1 is more significant. Results of the fit procedure show that this parameter basically influences behavior of the ratio $\gamma = {\rm Re}[t_C(q,\rho)]/{\rm Im}[t_C(q,\rho)]$ at $q \leq 1$ fm^{-1}. With μ_1 getting lower, ${\rm Re}[t_C(q,\rho)]$ increases, i.e., becomes more repulsive. This enhancement at low momenta transfer is accompanied by some increase in ${\rm Im}[t_C(q,\rho)]$ (i.e., diminishing in absolute value) meaning less absorption. Hence, the quantity γ being negative grows in its absolute value. This parameter is known to be responsible for filling in the minima of the differential cross sections at intermediate energies. Large negative values of γ at small q results in greater filling. Since the free t matrix gives a poor

description, predicting too low values in minima, a conspicuous modification of $t_C^0(q)$, especially its real part, becomes necessary. The value of μ_1 was chosen to be $\mu_1 = 1.2$ fm^{-1}, thus providing a better (as compared to $\mu_1 = \mu_2$) description of the elastic cross section for ^{40}Ca especially in the first minimum.

In order to make the description closer to experimental conditions, we included corrections for finite angular resolution due to binning of the data and for projectile multiple Coulomb scattering on different nuclei in the target. Because of the rapid oscillations of the p-nucleus cross sections with angle, it is better to parametrize the logarithm of the cross sections, rather than the cross sections themselves. The convenient form is

$$\ln\left[\frac{\sigma(\theta')}{\sigma(\theta)}\right] = \sqrt{\alpha}(\theta' - \theta) + \beta(\theta' - \theta)^2 , \tag{32}$$

where

$$\begin{aligned} \sqrt{\alpha} &= \sigma'/\sigma , \\ 2\beta &= \sigma''/\sigma - \alpha , \end{aligned} \tag{33}$$

σ' and σ'' being the first and the second derivatives of σ with respect to θ'. The expression for $\sigma(\theta')$ should be averaged over all the directions within the spectrometer bin angle $(2\delta\theta)$. After averaging [21] one has

$$\sigma_{\rm av}(\theta) = \sigma(\theta)\left[1 + \frac{(\delta\theta)^2}{6}(\alpha + 2\beta) + \frac{(\delta\theta)^4}{10}(\beta^2 + \alpha\beta + \alpha^2/12)\right] . \tag{34}$$

This expression must be corrected for the multiple scattering in the target with the effective thickness $t_0/\cos(\theta)$ ($t_0 = 0.15$ g/cm^2 in our case). The smearing procedure gives

$$\sigma_{\rm av}(\theta, t) = \sigma_{\rm av}(\theta)\,\frac{1}{\zeta}\exp\left(\frac{\langle\theta^2\rangle\alpha}{4\zeta^2}\right) , \tag{35}$$

where $\zeta^2 = 1 - \langle\theta^2\rangle\beta$. For $\langle\theta^2\rangle$, we used the expression from [45]:

$$\langle\theta^2\rangle = 0.157\,Z(Z+1)\,tA^{-1}(kv)^{-2} \times \ln(1.13\times 10^4 Z^{4/3}A^{-1}tv^{-2}) , \tag{36}$$

where k is the proton momentum in MeV/c and v is the proton velocity in the units of c, i.e., the light velocity.

In the case of ^{40}Ca those corrections have turned out to be fairly small. This is basically because the differential cross sections in the experiment EXP 760 [17] were measured with very small bin size $\simeq 0.2°$. On the other hand, the comparatively high proton energy 650 meV and a smooth general structure of the angular distribution for ^{40}Ca were also the reason why the angular averaging, which determines the corrections, did not produce any significant change. However, similar corrections in the case of ^{208}Pb are somewhat bigger reaching the value of a few percent.

Absolute normalization of the ^{40}Ca cross section of Ref. [17], used in the analysis, has been checked to be consistent with that of the elastic differential cross section for ^{40}Ca at 613 MeV measured at Saclay [46]. To do this, a small correction to the t matrix due to the energy difference was taken into account. This has been done by scaling down $\mathrm{Im}[t_C(q,\rho)]$ at 650 MeV in the proportion k_{613}/k_{650}, where k_{613} and k_{650} are the incident proton momenta for the corresponding energies. According to the optical theorem, this ratio basically describes the ratio of imaginary parts of the t matrices at low q. The values of the $\{a_i\}$ parameters providing the best fit to the ^{40}Ca data [34] are collected in Table I.

The central and spin-orbit t matrices in the momentum representation calculated with this set of parameters in the NN center-of-mass system are displayed in Fig. 1 by the solid lines. The former were evaluated at 650 MeV for the density $\rho = \rho_0$, where $\rho_0 = 0.159$ fm^{-3} is the nuclear matter density. The free t matrices of Ref. [18] at the same energy are shown by the dotted lines. From this comparison, one can conclude that significant modifications are required, the largest one is for $\mathrm{Re}[t_C(q)]$ at low q. This is a direct consequence of a poor description of the elastic scattering at 650 MeV obtained with the free t matrix, especially in the minima of the angular distribution. This is clearly seen in Fig. 2, where the results for the cross section $d\sigma/d\Omega$, analyzing power A_y, and the spin rotation parameter Q are presented. The data were taken from Refs. [17,46]. The results calculated with the effective and free interactions are depicted by the lines of the same type as in Fig. 1. The percent deviation between the theory and experiment $d = 200(\sigma^{\rm expt} - \sigma^{\rm th})/(\sigma^{\rm expt} + \sigma^{\rm th})$ %, shown in Fig. 3, displays in more detail the quality of the total best fit solution in the description of the differential cross section. Here, the agreement is mostly at the level of 10–15 % or better in the whole angular range including positions of the minima.

Returning to Fig. 1, one can point out that the overall repulsive contribution arising in $\mathrm{Re}[t_C(q,\rho)]$ due to the medium influence has been also obtained in the calculations [29,32] for the G matrix at energies up to 300 MeV and the τ matrix in the Watson formalism for higher energies [28]. This behavior is also in a qualitative agreement with what has been obtained for the phenomenological interaction of Ref. [16]. However, in our case, the enhancement of $\mathrm{Re}[t_C(q,\rho)]$ at low q resulting from the requirement of the best fit description of the elastic scattering data is much larger.

As to $\mathrm{Im}[t_C(q,\rho)]$, one can point out that the medium influence results in decreasing of its absolute value, the total quantity being negative. This means that the imaginary part of the optical potential which is determined by $\mathrm{Im}[t_C(q,\rho)]$ in the first-order approximation becomes less

TABLE I. Parameters of the effective isoscalar t matrix.

a_1	a_2 (MeV fm^3)	a_3	a_4 (MeV fm^3)	a_5	a_6 (MeV fm^3)
1.065	229.8	0.821	−32.39	0.942	3.638

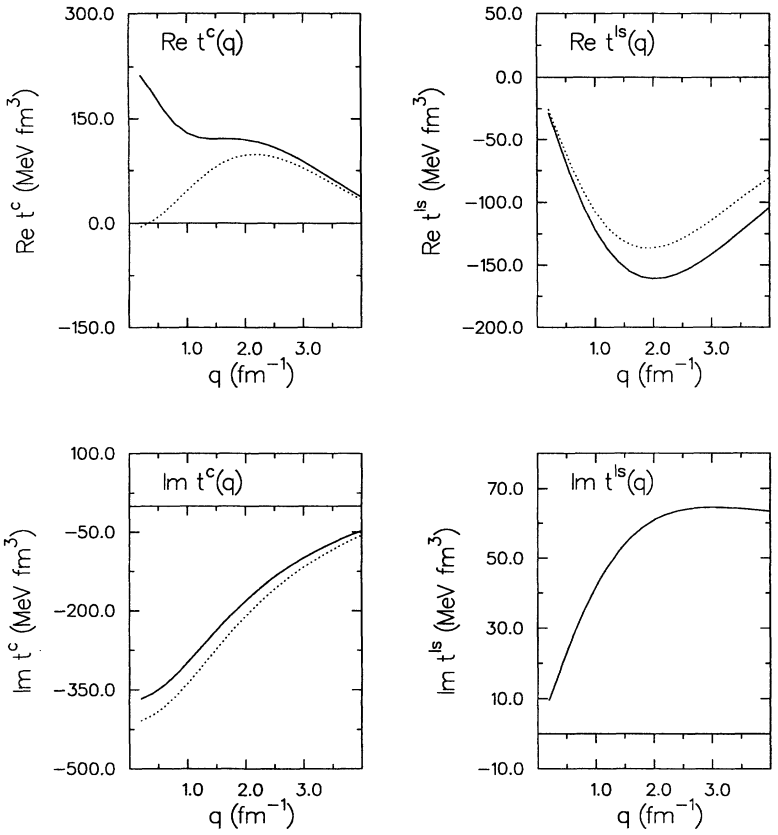

FIG. 1. Real and imaginary parts of the central $t_C(q)$ and spin-orbit $t_{LS}(q)$ isoscalar t matrices for NN scattering at 650 MeV. The solid lines show best fit solution including medium modifications [Eqs. (10)–(13), $\rho_0 = 0.159$ fm^{-3}], the dotted lines are the free t matrices of Ref. [18].

absorptive. That also implies decreasing of cross sections for inelastic channels. Such kind of behavior is compatible with the Pauli principle in the sense that the number of levels, accessible for rescattering in intermediate states, decreases implying a less negative imaginary part.

It is worth noting that ρ-dependent terms containing the coefficients a_2, a_4, and a_6 in Eqs. (10)–(13) are not the only ones which represent the medium influence. According to this parametrization at the zero density limit, the normalization factors a_1, a_3, and a_5 bear part of that influence too. Strictly speaking, they must be also ρ dependent. Therefore, the total contribution of both terms in each of the equations (10)–(13) determines the entire in-medium correction to the corresponding component of the free t matrix. In this respect, the negative sign of a_4 coefficient displayed in Table I does not imply any disagreement with the Pauli principle, as it could seem from the first sight.

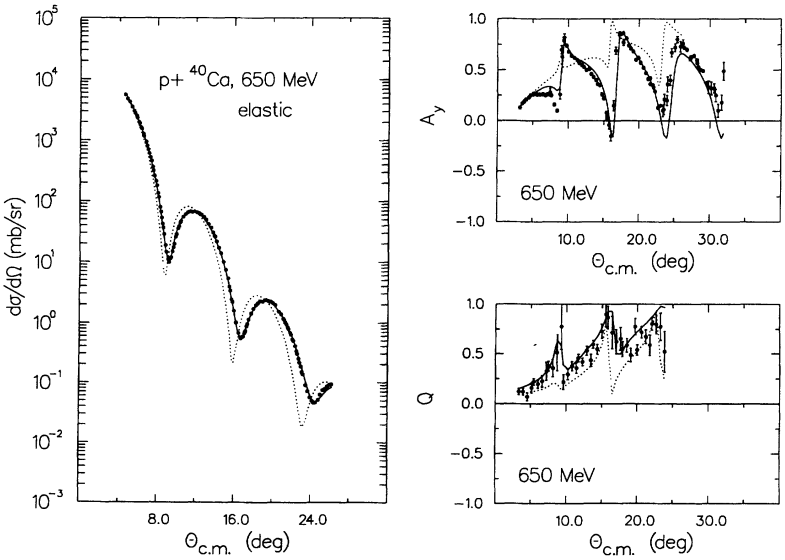

FIG. 2. The cross section for elastic p-^{40}Ca scattering (data from Ref. [17]), analyzing power A_y, and spin rotation parameter Q (data from Ref. [34]) at 650 MeV. The curves shown by the solid and dotted lines were calculated with the t matrices depicted in Fig. 1 by the lines of the same type.

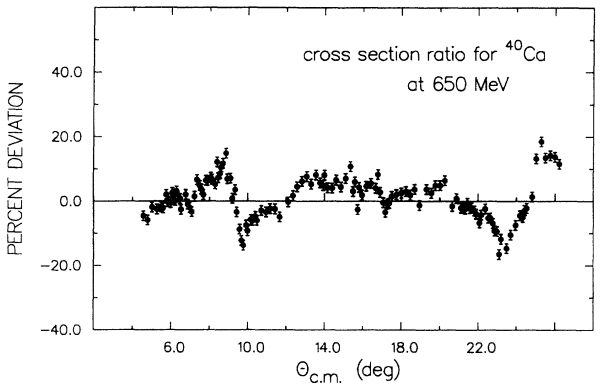

FIG. 3. Percent deviation between the experimental cross section for elastic p-^{40}Ca scattering at 650 MeV [17] and the cross section providing the best fit solution with the effective density dependent t matrix.

In order to examine more thoroughly our spin-orbit interaction, it is better to turn to the spin observables: the analyzing power A_y and the spin rotation parameter Q. As can be seen from Fig. 2, the medium corrections improve the description very substantially providing a good agreement with the experiment for A_y. Obviously, the data for Q at 650 MeV are not precise enough to make a critical judgment. This result for A_y confirms the conclusion made in Ref. [28] that within the nonrelativistic approach, it is really possible to achieve the quality of description of the spin observables comparable to that obtained in the best classic example—the analyzing power of ^{40}Ca at 500 MeV described within a relativistic model [47].

B. The neutron densities

We turn to a discussion of the results obtained for the neutron density distributions using the effective t matrix determined as was described above. First, we will demonstrate to what extent one can recover a neutron density from the so-called pseudodata using the inversion method outlined in Sec. III. These data are not a result of measurement, but are created by the density itself within the same theoretical framework which is used for analyzing real data. More specifically, we generated the pseudodata by assigning empirical error bars to the calculated cross section values and then randomizing them by means of a random number generator.

When inverting the pseudodata, different shapes of $\rho_n^0(r)$ were assumed including the HF densities and Fermi distributions with different values of shape parameters corresponding to the rms radii within 0.2 fm of the original neutron radius. Two examples of the pseudodata analysis for ^{208}Pb are shown in Figs. 4 and 5, where the extracted neutron densities are compared with the original ones. In the first case the pseudodata were generated by the HF density and inverted with $\rho_n^0(r)$ having the Fermi shape. In the second case, the Fermi function was the source and a Fermi-distribution with shifted shape parameters was used as $\rho_n^0(r)$. The expansion radius R_0

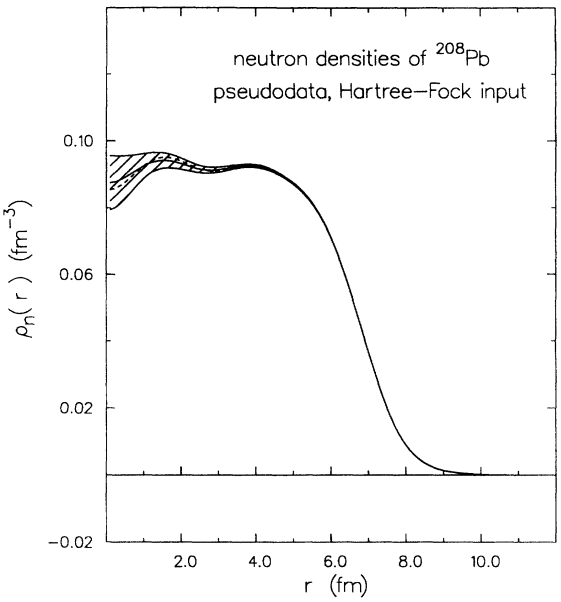

FIG. 4. Comparison of the best fit to pseudodata (the solid line) with the Hartree-Fock neutron density (the dashed line) which generated the pseudodata. The statistical error band for the best fit solution is shown by the shaded area.

was chosen to be 11 fm, the cutoff radius was 15 fm, and 10 expansion coefficients were included in the calculations, the same values being used in the analysis of real data. One can see that in both cases the extracted and original neutron densities are close enough to each other and are contained within the statistical error band shown in the plots by the hatched area.

Now, we turn to the examination of real data. The method for extraction of the neutron densities outlined in Sec. III was applied to the analysis of the elastic (pA)

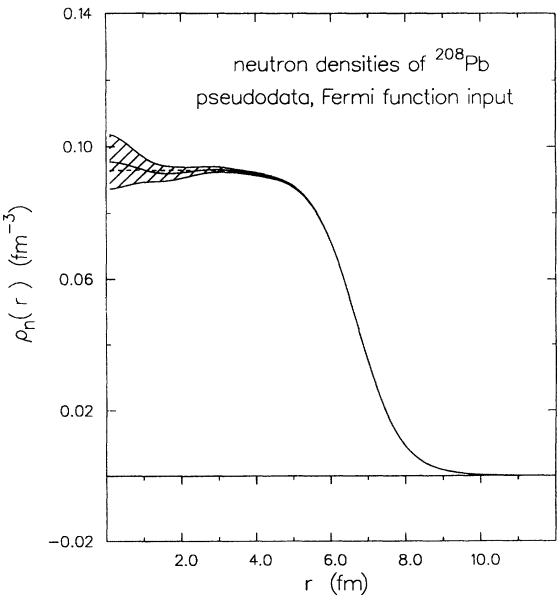

FIG. 5. Same as in Fig. 4 but for the Fermi function.

scattering cross sections and analyzing powers measured for ^{206,207,208}Pb. As an initial approximation $\rho_n^0(r)$, we used the HF neutron densities which have been calculated by us from the HF method with the Skyrme interaction SkM′, and the pairing included in the BCS approximation with the neutron pairing parameter $G_n = 20/A$. The proton pairing does not play any role for the closed shell Z=82. The odd isotope ^{207}Pb was treated in the filling approximation, which had been demonstrated to be good for heavy nuclei [48]. The sensitivity of the final results to the choice of $\rho_n^0(r)$ was fairly weak, provided the rms radius corresponding to $\rho_n^0(r)$ was kept fixed. Making use of the Fermi distribution with the same rms radius as $\rho_n^0(r)$ gave usually statistically equivalent results as compared to those obtained with the HF input.

Ten FB coefficients were included in the expansion of the correction term $\delta\rho_n(r)$. The last (10th) term carries the momentum $q_{10} = 10\pi/R_0 = 2.86$ fm^{-1}, which corresponds to the wavelength $\lambda_{10} = 2.20$ fm. The maximum momentum transfer attained in the experiment under consideration being 2.91 fm^{-1}. Separate calculations with $M = 11$ terms included and $R_0 \simeq 12$–13 fm, thus keeping the condition $q_{11} \leq q_{\max}$ fulfilled, gave essentially the same results. Nevertheless, the χ^2 solutions for $M = 10$ were more stable.

Another thing worth noting is that in addition to the isoscalar component found from the analysis of ^{40}Ca, we have tried to determine the isovector part of the effective t matrix, assuming the same form of parametrization with six new parameters. The isovector force was searched simultaneously with the neutron density parameters from an analysis of ^{208}Pb scattering data, keeping the isoscalar interaction fixed as it had been determined from ^{40}Ca. In this double fit procedure a switch was done after every three iterations from a force parameter search to a density parameter search and vice versa. We found that the best fit solution had a very shallow χ^2 minimum with respect to the isovector force parameters. The sensitivity to them was rather weak even in ^{208}Pb, thus providing a reason for omitting the isovector ρ-dependent terms.

In Fig. 6, results for the neutron $\rho_n(r)$ and matter $\rho_m(r) = \rho_n(r) + \rho_p(r)$ ($\rho_m \equiv \rho$) densities of ^{208}Pb, depicted with the statistical error bands, are compared to the HF predictions. The point proton density with its experimental uncertainty is also shown in the graph. The former was obtained by unfolding the charge density distribution of Ref. [43] with inclusion of the neutron charge distribution and effective spin-orbit charge density [36]. Both proton and neutron current densities calculated from the same HF approach were used to produce the spin-orbit charge distribution. Because of a considerable compensation between the terms containing proton and neutron magnetic moments, the overall spin-orbit contribution has turned out to be small, much smaller than that created by the neutron intrinsic charge distribution.

It is a common belief that mean field calculations fail to describe the charge densities of the lead isotopes in the central region of the nucleus, predicting too large values at $r = 0$ [1]. That discrepancy has been the subject of intensive theoretical studies. The inclusion of long-range

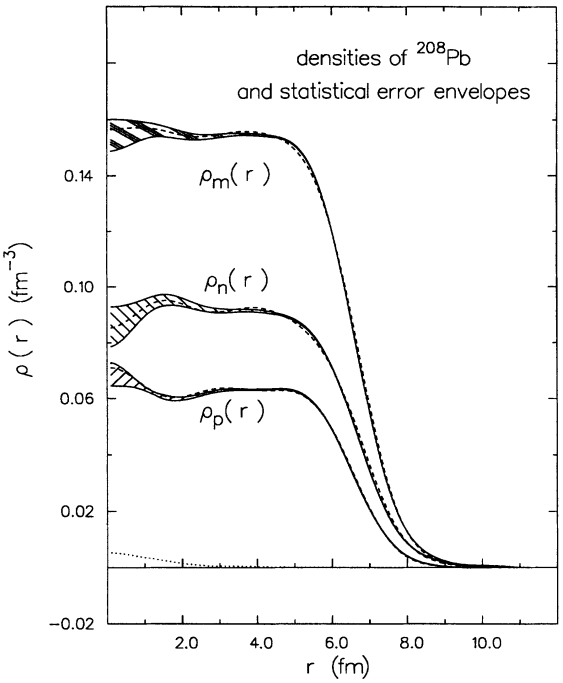

FIG. 6. Extracted neutron and matter densities for ^{208}Pb lying in the middle of the corresponding statistical error bands (the hatched areas). The HF proton, neutron, and matter densities are depicted by the dashed lines. The proton density obtained by unfolding the charge density of Ref. [43] is also shown with its statistical error envelope. The dotted line at the bottom is for the statistical error band obtained with the SOG method of Ref. [23].

correlations in the random-phase approximation [49] and short-range correlations as in Refs. [50,51] results in decreasing the occupation numbers for the proton $3s_{1/2}$ and $2d_{3/2}$ orbitals and thereby slightly improves the description. The contribution from the so-called dynamical pairing correlations [52] does not produce a drastic effect as well. However, the analysis [52] and this calculation show that a good description of $\rho_{\rm ch}(r)$ for ^{208}Pb can be achieved within the ordinary HF theory with the interaction SkM′ [10] without explicit modifications of the occupation probabilities. A good description has also been obtained with the QLM approach [13]. The influence of the range of the interaction on $\rho_{\rm ch}(r)$ was investigated in Ref. [54].

It is worth emphasizing here that the scattering quantities we consider are basically determined by the isoscalar variables (i.e., the sum of proton and neutron contributions). Therefore, our final conclusions about the neutron density distributions may be sensitive to the quality of the proton densities used in the analysis. In this respect, it was important to provide the best currently available charge densities and unfold them accurately with the fine features included. Our conclusions on the matter densities are much less dependent on the input charge densities.

The statistical error in $\rho_m(r)$ shown in Fig. 6 was calculated according to Eq. (31). It encloses all density distributions (within the limits of our model representa-

tion of the densities) which would be produced by the data normally distributed around each measured data point with a standard deviation. However, not every curve within the band describes a possible (normalized) physical solution. In order to judge whether a particular distribution is compatible with the data, the spatial correlations defined in Eq. (28) must be taken into account. The correlation function $D(r,r')$ determines the most probable deviation of the density $\rho(r)$ from the best fit solution at the point r, if $\rho(r')$ is fixed.

The quantity $\Delta\rho_n(r)$ associated with $\rho_n(r)$ includes also statistical errors in $\rho_{\rm ch}(r)$ as measured in the combined analysis [43] of electron scattering and muonic x-ray data. In the inner region, these errors are approximately twice as small as those we have determined for the matter density from the (pA) data.

Figure 7 shows the cross section and analyzing power A_y for the elastic (p-^{208}Pb) scattering. Besides the fitting curves depicted by the solid lines, the results obtained using the HF proton and neutron densities, and the effective t matrix are shown by the dashed lines. As can be seen, the quality of description is very good, perhaps even better than one could expect. Note that there were no adjustable parameters in this latter case, the effective t matrix having been fixed from the analysis of the

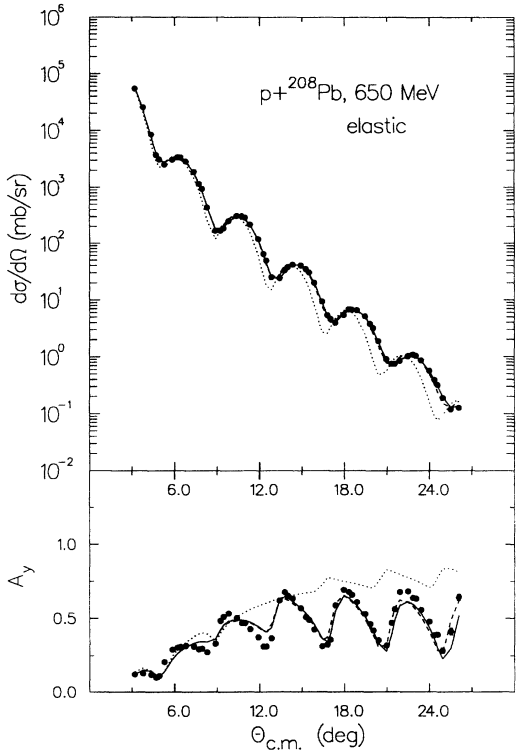

FIG. 7. Cross section and analyzing power for elastic p+^{208}Pb scattering at 650 MeV (the data are from Ref. [15]). The solid lines are for results obtained from fitting the neutron density parameters with the effective t matrix determined from the analysis of ^{40}Ca data. Use of this amplitude and the HF densities gives results depicted by the dashed lines. The dotted lines are for the case of using the HF densities and the free t matrix of Ref. [18].

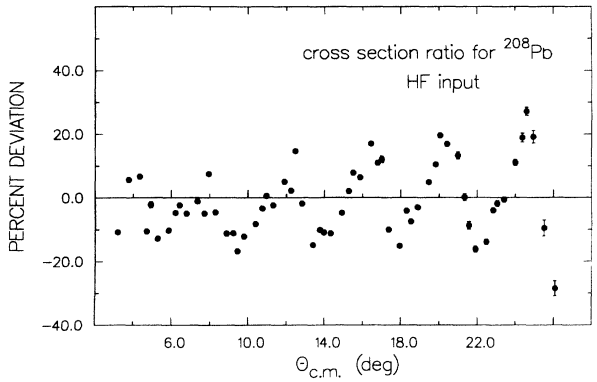

FIG. 8. Percent deviation between the experimental cross section for elastic p-^{208}Pb scattering at 650 MeV [15] and the cross section calculated using the HF densities and effective t matrix determined from the analysis of ^{40}Ca data.

^{40}Ca data. In order to discern fine features, we present in Fig. 8 the percent deviation (defined earlier in Sec. III A) between the cross sections calculated with HF densities and measured values with error bars being included. The comparison of the theoretical predictions with the experiment both for the proton density of ^{208}Pb in Fig. 6 and the elastic cross section in Figs. 7 and 8 provides a critical test for the effective t matrix determined and proves the consistency of the approach itself.

The percent deviation for the results obtained with the fitting procedure is shown in Fig. 9. One can see that the data are described at the level of 10% or better within the entire angular range.

The results for ^{206,207}Pb are qualitatively similar to those obtained for ^{208}Pb. They are presented in Figs. 10–13. The values of rms radii for the charge $r_{\rm ch}$ [43], proton r_p, neutron r_n, and matter r_m distributions are collected in Table II. The index HF corresponds to the HF result, and $r_p^{\rm un}$ is the radius for the unfolded charge (i.e., point proton) density, the statistical errors for r_n and r_m are indicated in parentheses.

One can conclude from Table II that the quantity $\Delta r_{np} \equiv r_n - r_p$ for ^{208}Pb is equal to 0.20 ± 0.04 fm. This

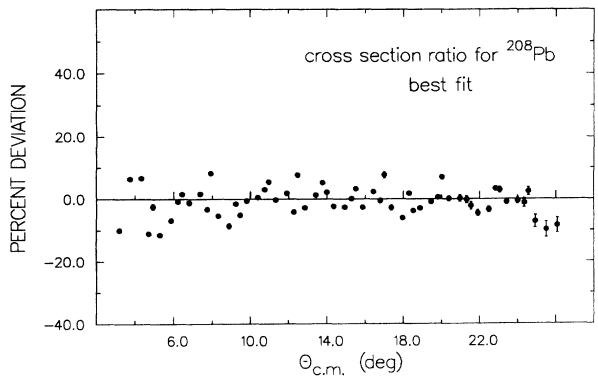

FIG. 9. Same as in Fig. 8 but for the best fit neutron density.

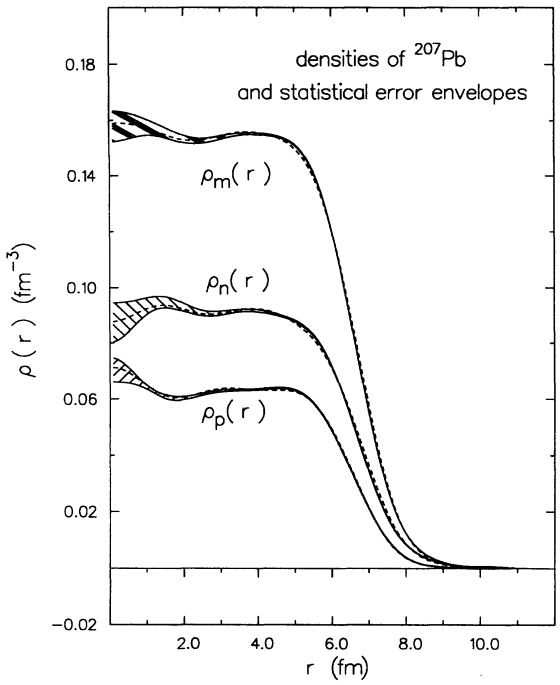

FIG. 10. Same as in Fig. 6 but for ^{207}Pb.

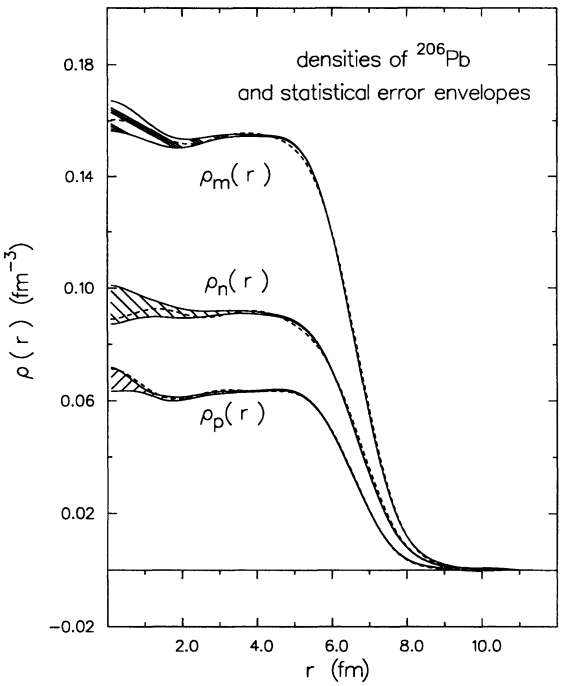

FIG. 12. Same as in Fig. 6 but for ^{206}Pb.

value is in a reasonable agreement with the result of Ref. [55] $\Delta r_{np} = 0.14 \pm 0.04$ fm obtained from the analysis of elastic p-^{208}Pb scattering at 0.8 GeV. The HF result for this quantity is 0.17 fm. The differences between neutron rms radii for ^{208}Pb-^{207}Pb, ^{208}Pb-^{206}Pb, and ^{207}Pb-^{206}Pb are 0.017, 0.029, and 0.012 (in fm), respectively, with the average statistical uncertainty less than 0.060 fm.

Another obvious source of uncertainty in the extracted densities is associated with the truncation of the FB series in Eq. (14). The overall contribution of higher harmonics which are not specified by the existing data is a model dependent error. By definition, we have

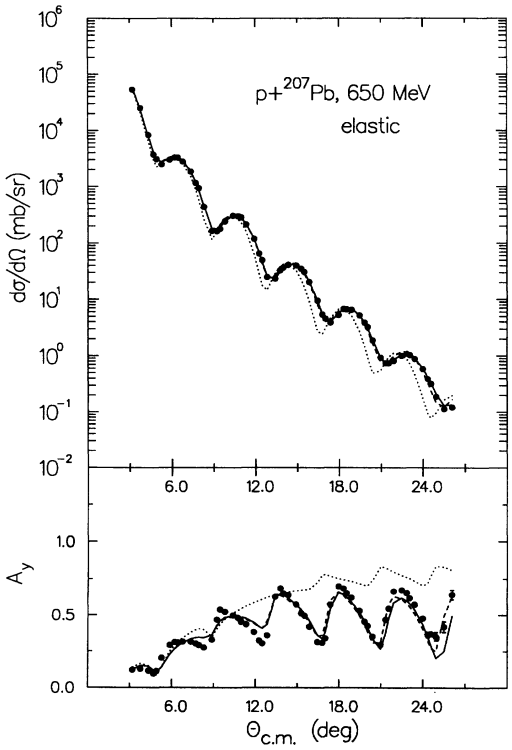

FIG. 11. Same as in Fig. 7 but for ^{207}Pb.

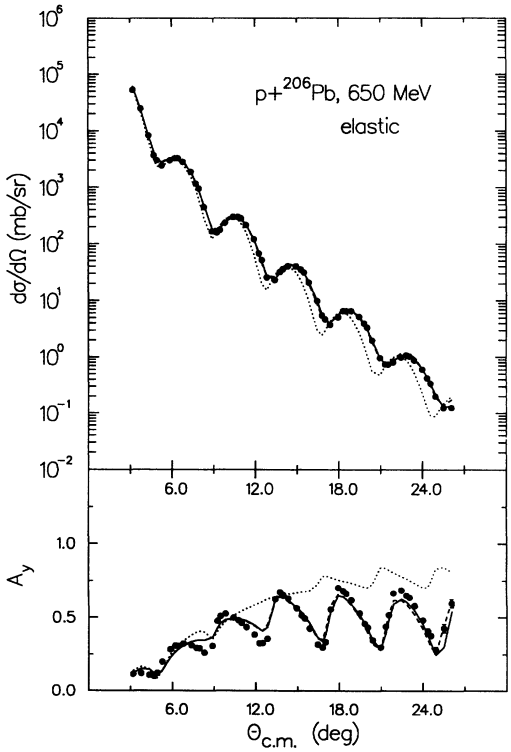

FIG. 13. Same as in Fig. 7 but for ^{206}Pb.

TABLE II. The rms charge, proton, neutron, and matter radii (in fm) with the statistical errors for r_n and r_m.

Nucleus	r_{ch}	r_p^{un}	r_p^{HF}	r_n^{HF}	r_m^{HF}	r_n	r_m
^{206}Pb	5.490(2)	5.445	5.439	5.596	5.534	5.626(45)	5.555(27)
^{207}Pb	5.497(2)	5.452	5.444	5.606	5.542	5.638(41)	5.565(25)
^{208}Pb	5.503(2)	5.458	5.449	5.617	5.551	5.655(42)	5.579(25)

$$\Delta\rho_n^M(r) = \left|\rho_n(r) - \sum_{m=1}^{M} C_m j_0(q_m r)\right| . \quad (37)$$

Perhaps, the easiest way to estimate this error is to evaluate the difference between the theoretical HF density $\rho_n^{HF}(r)$ and its M-term FB series, assuming that the HF result is a realistic approximation to the exact density. The latter has been demonstrated in the description of the p-^{208}Pb elastic cross section obtained with the HF result (Fig. 7) and in the comparison for the proton densities in Fig. 6.

The model error estimated for $M = 10$ and $R_0 = 11$ fm is shown in Fig. 14 together with the statistical error band. Only a smooth curve enclosing maxima of $\Delta\rho_n^M(r)$ is important. One can see that with ten coefficients included, the model error is less than the statistical envelope $\Delta\rho_n(r)$ in the region $r \leq 6$ fm and much less than $\rho_n(r)$ for $r \leq 11$ fm. Generally, the difference between the entire density and its FB expansion decreases as the number of expansion coefficients M increases. However, for too large M the magnitude of $\Delta\rho_n(r)$ can increase significantly if high harmonics unspecified by the data are introduced.

One can illustrate this point by showing how the statistical uncertainty $\Delta\rho_n(r)$ at the origin depends on M, the number of terms included in the FB expansion. Consequently, for $M = 9, 10, 11$, and 12 the values $\Delta\rho_n(0)$ were 5.6, 5.7, 6.8, and 13.2 in units of 10^{-3} fm^{-3}, respectively. One can see that a large increase in $\Delta\rho_n(0)$ begins for $M = 11$, and the search procedure breaks down for $M > 12$. As was said above, the condition for determination of the highest number of the FB terms $M = R_0 q_{max}/\pi$ yields $M = 10$ for $q_{max} = 2.91$ fm^{-1} and $R_0 = 11$ fm. The choice $M = 10$ looks optimal, because this keeps the statistical envelope narrow enough without introducing poorly determined coefficients. On the other hand, this does not lead to large model uncertainties (see Fig. 14). This character of the dependence of the statistical and model errors on M is very similar to what was obtained in Ref. [7] in the case of elastic electron scattering on ^{208}Pb.

For the purpose of comparison, we also employed the method of Ref. [23] to generate the statistical error envelope for $\rho_n(r)$ in ^{208}Pb. The neutron density was searched in the form

$$\rho_n(r) = b[\rho_n^0(r) + S\delta\rho_n(r)], \quad (38)$$

where $\delta\rho_n^0(r)$ is the initial approximation and $\delta\rho_n(r)$ is expanded in a sum of Gaussians (SOG):

$$\delta\rho_n(r) = (2\pi^{3/2}\gamma^3)^{-1} \sum_{i=1}^{W} Q_i (1 + 2c_i^2/\gamma^2)^{-1} \{\exp[-(r - c_i)^2/\gamma^2] + \exp[-(r + c_i)^2/\gamma^2]\}. \quad (39)$$

The positions c_i and strengths Q_i are chosen at random within the intervals $0 \leq c_i \leq R_0$, $0 \leq Q_i \leq 1$ with $R_0 = 11$ fm and $W = 12$. The width parameter γ restricts the high Fourier components that can appear in $\rho_n(r)$. Usually, the value of γ is assumed to be of the order of a lobe's width in the single-particle wave functions, that is typically 1.2–1.4 fm. The strength S of each perturbation $\delta\rho_n(r)$ is increased until the condition

$$|\sigma_\alpha(S) - \sigma_\alpha^{expt}| - |\sigma_\alpha(S)_{S=0} - \sigma_\alpha^{expt}| = \epsilon_\alpha \quad (40)$$

is satisfied at some data point. The coefficient b is reevaluated for each perturbation to ensure the correct normalization of ρ_n. With a sufficiently large number of random perturbations (we made 50), the error envelope $\Delta\rho_n(r)$ can be obtained.

To have a good starting approximation for $\delta\rho_n^0(r)$, we used the result of the FB analysis for ^{208}Pb described previously. With $\gamma = 1.39$ fm as in Ref. [23], the envelope $\Delta\rho_n(r)$ turned out to be very similar to that determined using the FB expansion, the difference being only about 10% at the origin. This quantity, obtained with the SOG method, is shown by the dotted line at the bottom of Fig. 6. The former is narrower than the one obtained in Ref. [23]. Although, the quality of the fit provided by $\delta\rho_n^0(r)$ is important, we think that the difference is most likely due to higher statistical accuracy in the elastic channel in the experiment E855 [15]. On the average, it is 0.7% for the cross section data, while for the data analyzed in Ref. [23] it is typically 1–2 %. When we doubled the values of the error bars in Eq. (40) and repeated the whole procedure with other parameter unchanged, the resulting statistical band turned out to be about twice as large, that is much closer to what was obtained in Ref. [23]. The dependence of $\Delta\rho_n(r)$ on the width γ was found to be significant. The former becomes larger

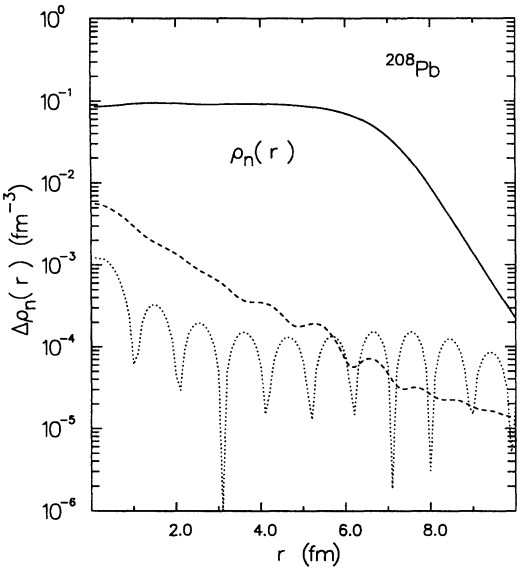

FIG. 14. Statistical error band (dashed line) and model error (dotted line) estimated for the ten-term FB series and the expansion radius $R_0 = 11$ fm. The HF neutron density of ^{208}Pb is shown by the solid curve.

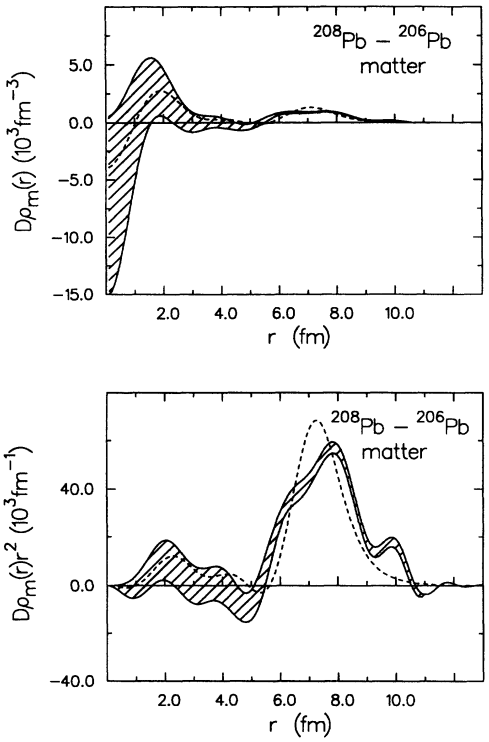

FIG. 15. The difference between matter densities of ^{208}Pb and ^{206}Pb with its statistical uncertainty shown by the hatched area. The HF prediction is drawn by the dashed line. The same quantities multiplied by the factor r^2 are displayed at the bottom.

with γ decreasing. In the instance of $\gamma = 1.0$ fm, we obtained $\Delta\rho_n(r)$ which was about twice as wide as that for $\gamma = 1.39$ fm.

Sometimes the SOG expansion is applied not to $\delta\rho_n(r)$, but to $\rho_n(r)$ itself [6]. In this case, $\Delta\rho_n(r)$ comprises not only statistical errors of the data, but also uncertainties associated with model assumptions about higher Fourier components of the density which are not sensed by the data. Those components are mostly controlled by the parameter γ in Eq. (39). One can note that in the FB expansion method used here $\Delta\rho_n(r)$ reflects only statistical fluctuations of the C coefficients included in the expansion. The high momentum components, which are not specified by the data, are excluded from the FB series. Being introduced in ρ_n^0 through the HF model, they do not contribute to $\Delta\rho_n(r)$.

C. The matter and neutron density differences

Here we present the results for the differences between the matter $D\rho_m(r)$ and neutron $D\rho_n(r)$ density distributions of the neighboring isotopes ^{206,207,208}Pb. Generally, such relative quantities are less sensitive to systematic errors and can be measured with greater accuracy than absolute measurements for a single nucleus. This allows one to study relative shifts produced by the addition of one or two particles in more detail. In particular, the density differences $D\rho_m(r)$ and $D\rho_n(r)$ for the isotopic pairs ^{208}Pb-^{206}Pb, ^{208}Pb-^{207}Pb (shown in Figs. 15–18) are especially sensitive to the successive addition of the $3p_{1/2}$ valent neutrons in creating the closed shell structure with N=126 if the shell model picture is assumed.

The results for the quantities $r^2 D\rho_{m,n}(r)$ are also displayed. The factor r^2, entering the normalization integral, was introduced to amplify the surface contribution and make it visibly more distinct. However, this factor can also enhance some deficiencies such as oscillations in the surface area. This peculiar structure does not have much physical significance. It is less pronounced in the matter distributions. To a large extent, the oscillations have come from the charge densities, where they apparently resulted from model assumptions on the form factor behavior at high q. The highest FB component included in the analysis [43] had the half wavelength $\simeq 0.7$ fm, too small to be directly specified by the data. The unfolding procedure used to obtain $\rho_p(r)$ from the charge densities has enhanced the oscillations further.

The statistical error envelopes for the density differences, shown in Figs. 15–18 by the hatched areas, were calculated by accounting for the statistical errors in each nucleus of a pair. In the case of neutron densities, the statistical errors in the charge densities were also included as they were determined in Ref. [43].

It is instructive to see to what extent normalization uncertainties of the measured cross sections can influence results for the extracted densities. In the experiment under consideration the absolute normalization errors were $\leq$7%. Therefore, we introduced the overall multiplication factors 0.93 and 1.07 for all the cross section data points (for ^{208}Pb) and inverted the data to see the effect. This dependence turned out to be significant for the densities. The matter rms radii changed their values within $\pm$0.09

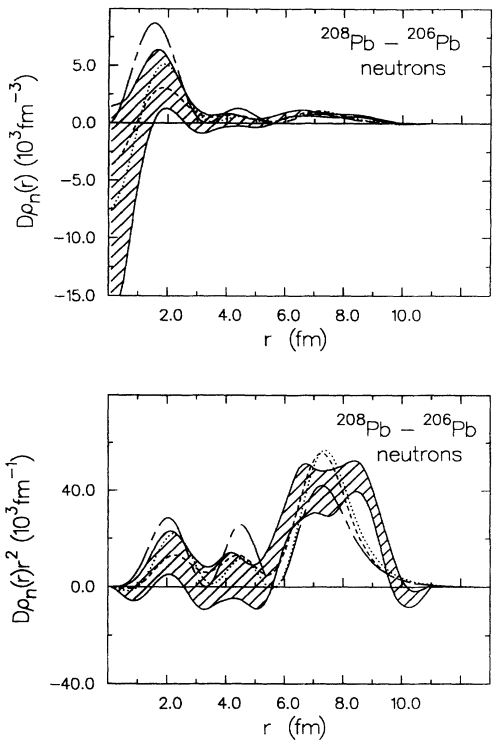

FIG. 16. The difference between neutron densities of ^{208}Pb and ^{206}Pb with its statistical uncertainty shown by the hatched area. The HF prediction with the parameter for neutron pairing $G_n = 20/A$ is drawn by the dashed line. The dotted curve is for $G_n = 0$. The broken solid line describes the contribution from the $3p_{1/2}$ neutrons in ^{208}Pb normalized to 2. The same quantities multiplied by the factor r^2 are displayed at the bottom.

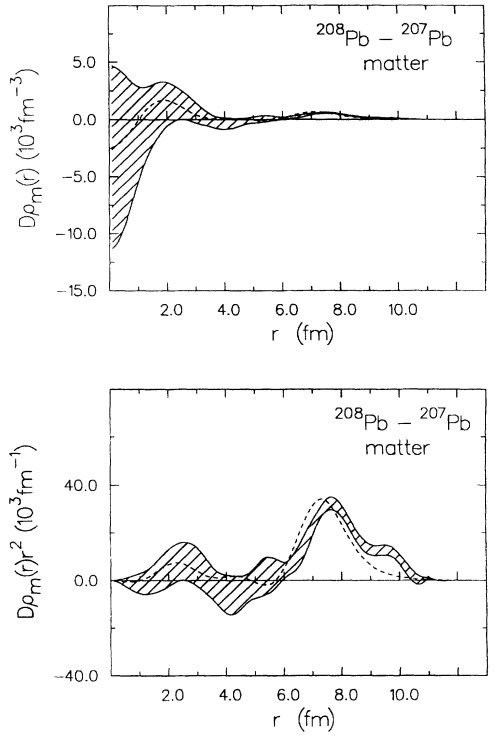

FIG. 17. Same as in Fig. 15 but for the difference ^{208}Pb-^{207}Pb.

fm, i.e., ≃2%. Another type of calculations were also done by varying the absolute normalization to minimize χ^2. The value 1.037 found from the search procedure lies within the normalization uncertainty range.

Although the density distributions and their radii for individual nuclei depend strongly on the normalization, the density differences between two isotopes are weakly sensitive to its precise value if identical normalization shifts are made for both nuclei. For a 5% shift this is illustrated in Fig. 19, where the neutron density difference between ^{208}Pb and ^{207}Pb is seen to be very small from that shown in Fig. 18. The sensitivity of the density differences to the relative normalization uncertainty between the three sets of data, which was ≃2 %, has been found to be much more significant. This is illustrated in Fig. 19 for the case of a 2% shift between normalizations of ^{208}Pb and ^{207}Pb. It influences mostly the amplitude of the oscillations. Shown in Fig. 19 the sensitivity to the uncertainties in the measured scattering angle ≃0.05° is seen to be of minor importance for the density differences.

The results for $D\rho_{m,n}(r)$ are compared to the predictions of the HF theory with the interaction SkM′ and pairing included. The single-particle contribution from the $3p_{1/2}$ neutron orbital normalized to two is also shown (Fig. 16). One can see a significant deviation from the

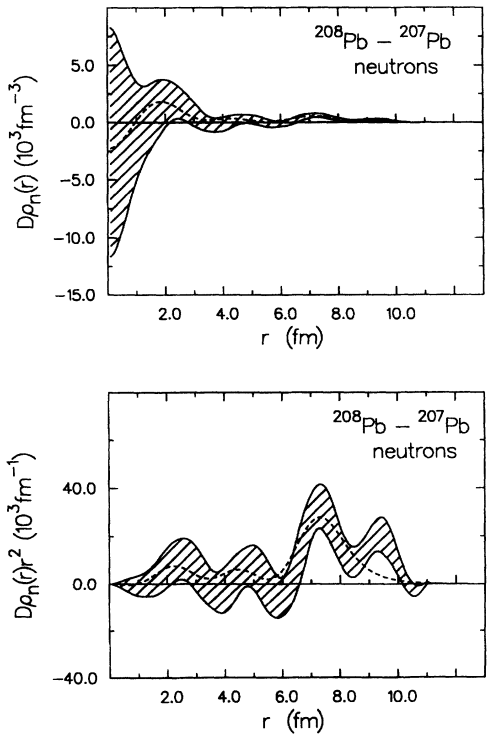

FIG. 18. The difference between neutron densities of ^{208}Pb and ^{207}Pb with its statistical uncertainty shown by the hatched area. The HF prediction is drawn by the dashed line. The same quantities multiplied by the factor r^2 are displayed at the bottom.

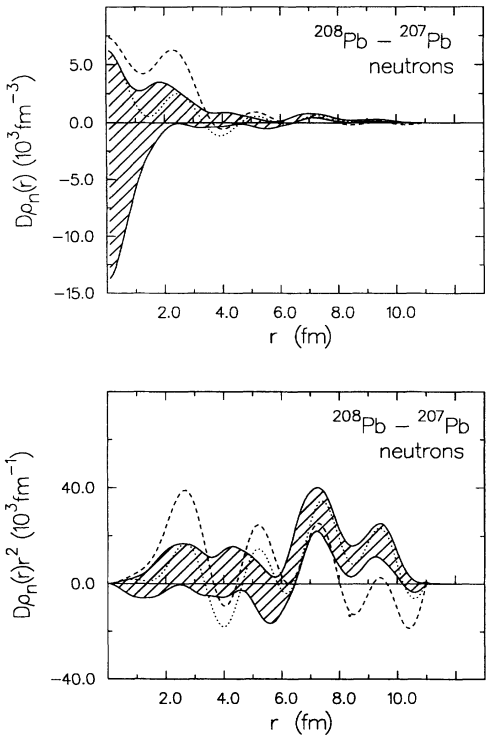

FIG. 19. The difference between neutron densities of ^{208}Pb and ^{207}Pb calculated using a 5% shift in the absolute normalization values for both nuclei. This difference is enclosed by the statistical uncertainties displayed by the hatch area. It must be compared to that shown in Fig. 18. T dashed line is for the case of 2% difference in the normalization between two isotopes. The dotted curve is the result obtained with the angle shift 0.05° in the differential cross sections and analyzing powers for both nuclei.

single-particle picture. It can be attributed to a polarization effect produced by the $3p_{1/2}$ neutrons due to their substantial presence in the inner region of the nucleus [53]. The HF result includes a part of the core polarization, owing to the self-consistency of the mean nuclear field.

The behavior of $D\rho_{m,n}(r)$ in the surface is mostly determined by bulk properties of the mean field and is not very sensitive to details of the NN force. Whereas in the inner region, the density differences depend strongly on fine properties of the NN interaction and, in the case of ^{206}Pb, on the strength of neutron pairing correlations. This sensitivity is demonstrated in Fig. 16 for two values of the pairing constant $G_n = 20/A$ and $G_n = 0$. From Figs. 15–18 one can conclude that, on the whole, the present version of the HF theory describes the differences $D\rho_{m,n}(r)$ reasonably well. There are some discrepancies in the description of minor features.

Closing this section, we can note that our computer code for the χ^2 fit procedure has been written in such a way as to make a search of the parameters for the t matrix and densities on the same basis. It also allows a switch from one type of a search to another. Normally, the convergence was very good providing the 10^{-3} relative accuracy in the χ^2 values in 5–6 iterations. To calculate the cross sections and spin observables, we used the codes ALLWORLD [56] and DWBA70 [57] which we have modified and made much faster in the elastic channel.

V. SUMMARY

We have presented the approach in which two major issues are addressed. The first one concerns the medium modifications in the interaction of incident protons with target nucleons at intermediate energies. The second one is directed to obtaining the information on the matter and neutron ground state densities by inverting data for the elastic p-nucleus scattering with statistical and model errors in the final results being estimated. Certainly, our results are model dependent. Truly model-independent determination of the density distributions is impossible. Clearly, the statistical error bands should not be understood as embracing all conceivable densities providing fits of a similar quality. They only show how the corrections to the HF densities, including low Fourier components determined by the data, fluctuate due to experimental error bars. The high-frequency components, being introduced through the HF model, do not contribute to our statistical error bands.

Using the fact of a considerable compensation between terms quadratic in the scattering amplitude, we treated the effective nuclear potential to the first order in the t matrix and single-particle densities. Medium corrections to the impulse approximation were included in this first-order structure by introducing density dependent terms. The choice of parametrization for the ρ dependence was motivated to a large extent by the hypothesis [20] on the universal renormalization of meson and nucleon masses in the nuclear medium. Using this idea, mass parameters of the free t matrix were treated as ρ-dependent quantities to generate the gross structure of the density dependent terms. The parameters for the isoscalar central and spin-orbit components have been determined by fitting the cross section and spin observable data for p-^{40}Ca elastic scattering at 650 MeV, the single-particle densities being known very well in this case.

The resulting density modifications show an enhancement of the repulsive contribution for the real central part of the isoscalar t matrix, especially at small q, and make the imaginary part less absorptive, the latter being in accordance with the Pauli principle.

The effective t matrix we have obtained can be also used for the description of inelastic scattering and other reactions at energies close to 650 MeV. The procedure could be straightforwardly extended to other energies within the range 100–1000 MeV where good scattering data exit.

To determine the neutron and matter densities in ^{206,207,208}Pb, we have extended the method of Ref. [21] originally proposed for the extraction of charge densities. A searched neutron density was presented in the form $\rho_n(r) = \rho_n^{\rm HF}(r) + \delta\rho_n(r)$, where the main term $\rho_n^{\rm HF}(r)$ was calculated with the HF theory and the correction $\delta\rho_n(r)$ was expanded in the FB series. Measured quantities were linearized with respect to $\delta\rho_n/\rho_n^{\rm HF}$, and the

expansion coefficients were determined from a system of linear equations obtained from the χ^2 minimum condition. The inversion procedure gives the so-called error matrix allowing one to calculate the density correlation matrix and statistical error band for the densities. The typical statistical uncertainties in the matter densities were about 5.6×10^{-3} fm^{-3} at $r = 0$, vanishing rapidly away from the center. The errors in $\rho_n(r)$ are approximately 17% larger (at the center) due to incorporated statistical uncertainties in the charge densities.

Another source of errors in the densities is the unknown behavior of measured quantities at q beyond $q_{\max}$, or equivalently an unknown contribution of higher harmonics not included in the FB series. We have estimated this unavoidable uncertainty with the help of theoretical densities and found that with 10 coefficients included and the expansion radius 11 fm (corresponding to $\lambda_{\min} = 2.2$ fm) this model error is generally less than the statistical uncertainty for $r \leq 6$ fm, being much less than the density itself for $r \leq 11$ fm.

We also examined the sensitivity of the results to absolute normalization of the cross sections by changing the normalization factor within the experimental uncertainty range ± 7 %. This dependence has been found to be significant for the densities. However, it was not that important for the density differences between two isotopes if identical changes of the normalization were done for both of them. Calculations with the normalization factor being free to minimize χ^2 resulted in a value (1.037) which is enclosed in the uncertainty range. We have also estimated the sensitivity of the density differences to the relative normalization uncertainties $\simeq 2$ % and errors in the scattering angle $\simeq 0.05°$.

In the HF theory we used the Skyrme-type interaction SkM′ and the constant of neutron pairing was chosen to be $20/A$. On the whole, the results for the density distributions, their differences in isotopic pairs, and rms radii are described by this version of the HF theory fairly well.

ACKNOWLEDGMENTS

We would like to express our deep gratitude to G.W. Hoffmann for communicating ^{40}Ca and ^{208}Pb cross section data at 650 MeV to us and several very useful discussions associated with them. We are also grateful to L. Ray for providing us ^{40}Ca data on cross section and spin observables. The help from M.A. Franey and A. Sethi in the beginning of this work is deeply appreciated. Our thanks are due M. Hughes and other members of Technical support group of the Minnesota Supercomputer Institute for numerous consultations and help. This work was supported by grants from the U.S. Department of Energy and the Minnesota Supercomputer Institute.

[1] B. Frois and C. N. Papanicolas, Annu. Rev. Nucl. Part. Sci. **37**, 133 (1987).
[2] C. J. Batty *et al.*, in *Advances in Nuclear Physics*, edited by J. W. Negele and E. Vogt (Plenum, New York, 1989), Vol. 19, p. 1.
[3] J. M. Cavedon *et al.*, Phys. Rev. Lett. **58**, 195 (1987).
[4] J. Friedrich and F. Lenz, Nucl. Phys. **A183**, 523 (1972).
[5] J. Borysowicz and J. H. Hetherington, Phys. Rev. C **7**, 2293 (1973).
[6] I. Sick, Phys. Lett. **44B**, 62 (1973); Nucl. Phys. **A218**, 509 (1974).
[7] J. L. Friar and J. W. Negele, in *Advances in Nuclear Physics*, edited by M. Baranger and E. Vogt (Plenum, New York, 1975), Vol. 8, p. 219.
[8] V. E. Starodubsky, V. R. Shaginyan, and Yu. I. Sholokhov, Yad. Fiz. **25**, 306 (1977) [Sov. J. Nucl. Phys. **25**, 167 (1977)].
[9] L. Ray, Phys. Rev. C **19**, 1855 (1979).
[10] J. Bartel *et al.*, Nucl. Phys. **A386**, 79 (1982).
[11] F. Tondeur *et al.*, Nucl. Phys. **A420**, 297 (1984).
[12] V. A. Khodel and E. E. Saperstein, Phys. Rep. **92C**, 183 (1982).
[13] E. E. Saperstein and V. E. Starodubsky, Phys. Elem. Part. Atom. Nucl. (Dubna, USSR) **20**, 293 (1989).
[14] G. Jacob and Th. A. J. Maris, Rev. Mod. Phys. **38**, 121 (1966).
[15] A. M. Mack *et al.* (unpublished).
[16] J. J. Kelly *et al.*, Phys. Rev. C **43**, 1272 (1991); **44**, 2602 (1991).
[17] G. W. Hoffmann, University of Texas at Austin Progress Report, 1984 (unpublished).
[18] M. A. Franey and W. G. Love, Phys. Rev. C **24**, 1073 (1981); **31**, 488 (1985).
[19] G. E. Brown, Nucl. Phys. **A488**, 659c (1988).
[20] G. E. Brown and M. Rho, Phys. Rev. Lett. **66**, 2720 (1991).
[21] J. L. Friar and J. W. Negele, Nucl. Phys. **A212**, 93 (1973).
[22] V. E. Starodubsky and V. R. Shaginyan, Yad. Fiz. **30**, 55 (1979) [Sov. J. Nucl. Phys. **30**, 28 (1979)]; V. E. Starodubsky and V. R. Shaginyan, Len. Nucl. Phys. Inst. Report No. LNPI-296, 1976 (unpublished).
[23] L. Ray, W. R. Coker, and G. W. Hoffmann, Phys. Rev. C **18**, 2641 (1978).
[24] J. A. McNeil, J. Shepard, and S. J. Wallace, Phys. Rev. Lett. **50**, 1443 (1983); B. C. Clark *et al.*, *ibid.* **50**, 1644 (1983).
[25] J. A. Tjon and S. J. Wallace, Phys. Rev. C **36**, 1085 (1987).
[26] L. Ray and G. W. Hoffmann, Phys. Rev. C **31**, 538 (1985).
[27] H. F. Arellano, F. A. Brieva, and W. G. Love, Phys. Rev. C **41**, 2188 (1990); R. Crespo, R. C. Johnson, and J. A. Tostevin, *ibid.* **41**, 2257 (1990); Ch. Elster *et al.*, *ibid.* **41**, 814 (1990).
[28] L. Ray, Phys. Rev. C **41**, 2816 (1990); L. Ray, talk at the International Conference on Spin and Isospin in Nuclear Interactions, Telluride, CO, 1991 (unpublished).
[29] L. Rikus, K. Nakano, and H. V. von Geramb, Nucl. Phys. **A414**, 413 (1984); L. Rikus and H. V. von Geramb, *ibid.* **A426**, 496 (1984).
[30] G. D. Alkhazov, S. L. Belostotsky, and A. A. Vorobyov,

Phys. Rep. **42C**, 89 (1978).
[31] V. E. Starodubsky, Yad. Fiz. **29**, 884 (1979) [Sov. J. Nucl. Phys. **29**, 454 (1979)]; E. E. Saperstein and V. E. Starodubsky, *ibid.* **30**, 70 (1979) [**30**, 36 (1979)]; **46**, 69 (1987), [**46**, 44 (1987)].
[32] K. Nakayama and W. G. Love, Phys. Rev. C **38**, 51 (1988).
[33] K. M. Watson, Phys. Rev. **89**, 575 (1953).
[34] E. Bleszynski *et al.*, Phys. Rev. C **37**, 1527 (1988); the spin observable data from C. A. Whitten were communicated to us by L. Ray.
[35] I. Sick *et al.*, Phys. Lett. **88B**, 245 (1979).
[36] W. Bertozzi *et al.*, Phys.Lett. **41B**, 408 (1972).
[37] J. W. Negele, Rev. Mod. Phys. **54**, 913 (1982).
[38] P. Quentin and H. Flocard, Annu. Rev. Nucl. Part. Sci. **28**, 523 (1978).
[39] G. E. Brown, A. Sethi, and N. M. Hintz, Phys. Rev. C **44**, 2653 (1991).
[40] N. M. Hintz, A. M. Lallena, and A. Sethi, Phys. Rev. C **45**, 1098 (1992).
[41] N. M. Hintz *et al.*, Nuclear Structure Studies at Intermediate Energies, Progress Report 1991–1992, University of Minnesota, p. 40 (unpublished).
[42] P. R. Bevington, *Data Reduction and Error Analysis for the Physical Sciences* (McGraw-Hill, New York, 1969).
[43] H. Euteneuer, J. Friedrich, and N. Voegler, Nucl. Phys. **A298**, 452 (1978).
[44] B. Dreher *et al.*, Nucl. Phys. **A235**, 219 (1974).
[45] H. A. Bethe and J. Ashkin, in *Experimental Nuclear Physics*, edited by E. Segre (Wiley, New York, 1953), Vol. 1, p. 304.
[46] G. Bruge, Saclay Report No. DPh-N/ME/78-1, 1978 (unpublished); L. Ray, private communication.
[47] N. Ottenstein, S. J. Wallace, and J. A. Tjon, Phys. Rev. C **38**, 2272 (1988); **38**, 2289 (1988).
[48] A. E. Barzakh and V. E. Starodubsky, Yad. Fiz. **45**, 45 (1987) [Sov. J. Nucl. Phys. **45**, 28 (1987)].
[49] J. Dechargé and L. Šips, Nucl. Phys. **A407**, 1 (1983).
[50] V. R. Pandharipande, C. N. Papanicolas, and J. Wambach, Phys. Rev. Lett. **53**, 1133 (1984).
[51] M. Jaminon, C. Mahaux, and H. Ngô, Nucl. Phys. **A440**, 228 (1985); C. Mahaux *et al.*, Phys. Rep. **120C**, 1 (1985).
[52] L. Bennour *et al.*, Phys. Rev. C **40**, 2834 (1989).
[53] J. Friedrich, Phys. Rev. C **33**, 2215 (1986).
[54] J. Martorell and D. W. L. Sprung, Z. Phys. **A298**, 153 (1980); F. Garcias, M. Casas, and J. Martorell, Nucl. Phys. **A490**, 348 (1988).
[55] G. W. Hoffmann *et al.*, Phys. Rev. C **21**, 1488 (1980).
[56] J. Carr, F. Petrovich, and J. Kelly, computer code ALLWORLD (unpublished).
[57] R. Schaeffer and J. Raynal, computer code DWBA70 (modified); J. Raynal, Nucl. Phys. **A97**, 572 (1967).